

Dissipative structures: From reaction-diffusion to chemo-hydrodynamic patterns

M. A. Budroni^{a)} and A. De Wit^{b)}

Nonlinear Physical Chemistry Unit, Service de Chimie Physique et Biologie Théorique, Université libre de Bruxelles (ULB), CP 231 - Campus Plaine, 1050 Brussels, Belgium

(Received 17 June 2017; accepted 7 September 2017; published online 26 September 2017)

The interplay of reaction and diffusion processes can trigger localized spatiotemporal patterns when two solutions containing separate reactants A and B of an oscillating reaction are put in contact. Using the Brusselator, a classical model for chemical oscillations, we show numerically that localized waves and Turing patterns as well as reaction-diffusion (RD) patterns due to an interaction between these two kinds of modes can develop in time around the reactive contact zone depending on the initial concentration of reactants and diffusion coefficients of the intermediate species locally produced. We further explore the possible hydrodynamic destabilization of an initially buoyantly stable stratification of such an $A + B \rightarrow$ oscillator system, when the chemical reaction provides a buoyant periodic forcing via localized density changes. Guided by the properties of the underlying RD dynamics, we predict new chemo-hydrodynamic instabilities on the basis of the dynamic density profiles which are here varying with the concentration of one of the intermediate species of the oscillator. Nonlinear simulations of the related reaction-diffusion-convection equations show how the active coupling between the localized oscillatory kinetics and buoyancy-driven convection can induce pulsatile convective fingering and pulsatile plumes as well as rising or sinking Turing spots, depending on the initial concentration of the reactants and their contribution to the density. *Published by AIP Publishing.* [<http://dx.doi.org/10.1063/1.4990740>]

When maintained out-of-equilibrium, physico-chemical systems can spontaneously self-organize in so-called dissipative structures featuring space and/or time symmetry breaking. As an example, convective currents can develop in fluids in the presence of given gradients of temperature or of concentration. In the wide class of the so-called reaction-diffusion (RD) systems, temporal oscillations, traveling waves, or stationary Turing patterns in which the variables are modulated in space can also emerge in the presence of non-equilibrium constraints. Thanks to the pioneering work of Prigogine, the conditions of emergence of such spatio-temporal dynamics are nowadays well understood. Important theoretical understanding of the properties of such dissipative structures has benefited from progress using the Brusselator model, a simple autocatalytic chemical model introduced by Prigogine and Lefever in 1968. The simplicity and genericity of this model still allow to deepen our understanding of chemo-hydrodynamic patterns resulting from the interplay between reaction-diffusion structures and convective motions.

I. INTRODUCTION

Far-from-equilibrium, self-organized systems can evolve towards increased complexity, order and coordinated collective behaviours as well as chaotic dynamics to name a few. Chemical oscillations of concentrations in both inorganic and

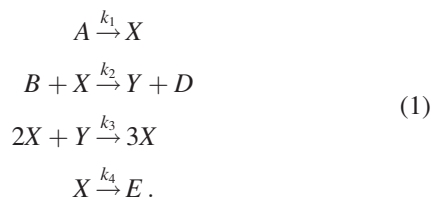
biological systems represent one of the most fascinating examples of such complexity in time. Traveling waves and stationary Turing structures in which the variable of interest is modulated in space are other examples of the genuine capacity of physico-chemical systems to organize themselves spontaneously when maintained out of equilibrium. Thanks to the pioneering work of Prigogine and of the members of the Brussels School of Thermodynamics, the spontaneous emergence of order out of disorder has been rationalized within an extended theory of non-equilibrium thermodynamics taking into account far-from-equilibrium conditions where the so-called *dissipative structures* can induce spontaneous space and time symmetry breaking.^{1,2}

In this context, Prigogine and co-workers made fundamental theoretical progress including, among others, the formulation and detailed analysis of the first chemical model giving a thermodynamically consistent description of oscillations and spatiotemporal structures in a chemical system, the Brusselator model.²⁻⁵ The simplicity of the Brusselator has allowed analytical understanding and interpretation of the conditions necessary to induce non-equilibrium instabilities. As such, it has played an important role in deciphering complex dynamics in experimental systems such as oscillations and waves observed in the more complex Belousov-Zhabotinsky (BZ)^{6,7} reaction or Turing patterns first discovered with the chlorite-iodide-malonic acid (CIMA) reaction.⁸ This model is still used to understand analytically the key mechanisms of pattern formation in spatially extended systems, not only in chemistry but more generally in the wide class of the so-called reaction-diffusion (RD) systems.

^{a)}Electronic mail: mbudroni@ulb.ac.be

^{b)}Electronic mail: adewit@ulb.ac.be

The kinetic scheme of the irreversible Brusselator model reads^{2,3,5}



This is a typical example of a *positive feedback* system,² where $\{k_i, i = 1, 4\}$ represents the set of rate constants, $\{A, B\}$ are the initial reactants, $\{D, E\}$ are waste products, and $\{X, Y\}$ the reaction intermediates with X the autocatalytic species. This reaction set embeds the minimal conditions for the onset of chemical oscillations, namely the production of at least two oscillatory intermediates, one non-linear step featuring the autocatalytic production of one intermediate (clock step), a mechanism by which the amplification of this autocatalyst is limited and the chemical clock reset.

The Brusselator has largely been used for the study of reaction-diffusion (RD) dynamics in conditions where the initial reactants are homogeneously distributed.^{2,9} The presence of gradients in the concentrations of one of the initial reactants A and B has also been exploited as a means to induce localized RD structures in the same system.^{2,9-14} This can typically occur in experiments when non uniform profiles of concentrations of the main reactants result from the feeding of the system from the sides.^{8,9,14-18} These concentration gradients can lead to localized waves (such as excyclons for instance^{19,20}), Turing patterns spatially confined in a part of the reactor^{8,14-18} or coexistence in different parts of the reactor of waves and Turing patterns.¹⁸ In parallel, the Brusselator has also been largely used to decipher new spatio-temporal dynamics arising from the interplay between Turing and Hopf modes in the vicinity of a codimension-two bifurcation point in conditions where the concentration of reactants A and B is uniform in space.²¹⁻²⁴

Recently, we also analyzed pattern localization in $A + B \rightarrow$ oscillator systems, in which two gels, each of them containing different reactants A or B of an oscillatory reaction, are put in contact in a closed reactor.²⁵ Once the gels are in contact, the reactants can diffuse and fuel locally the nonlinear chemical processes. This problem is the generalisation to autocatalytic and excitable kinetics of the largely studied $A + B \rightarrow C$ front case.²⁶ In the context of the $A + B \rightarrow$ oscillator system, we used the Brusselator model to explore analytically the spatio-temporal deployment of waves and of stationary Turing structures in localized zones of the reactor.²⁵ We provided a general classification of the possible dynamics and spatial coexistence of different instability modes as a function of the ratio of the initial concentration of the two reactants and the ratio of diffusion coefficients of the reaction intermediates. Depending on the values of parameters, the system can exhibit either localized waves or a combination of localized stationary Turing structures and Hopf modes expanding in space around the codimension-two Turing-Hopf (CTH) point.

An initial objective of this analysis was to understand whether such $A + B \rightarrow$ oscillator RD patterns could be used as a localized oscillatory forcing of convective hydrodynamic instabilities in a double-layer liquid system in the absence of a gel. Concentration gradients triggered by RD processes can indeed trigger unfavorable mobility gradients (i.e., here *in-situ* density gradients) which, in turn, can induce convection.²⁷ An initially buoyantly stable stratification of a less dense reactive solution on top of a denser one in the gravity field can then undergo a convective instability mediated by chemical processes when the reaction locally produces either a product of different density or having a different diffusion coefficient than the one of the initial reactants.²⁷⁻³² The resulting hydrodynamic patterns show convective fingers or plumes growing vertically.

Simple kinetic schemes of the $A + B \rightarrow C$ type have been largely studied in this context. They have been shown to drastically affect the space-time morphology of convective dynamics.^{29,30,32} In particular, such reactions are able to break the up-down symmetry of the convective patterns^{30,32} or can generate different chemo-hydrodynamics structures in the course of time.³² Nevertheless, in such $A + B \rightarrow C$ systems, the RD density profiles underlying the onset of convective patterns are asymptotically self-similar³³ and cannot feature transverse spatial breaking of symmetry in the absence of flows or complex temporal dynamics.

The goal of this article is to move a step further in complexity and probe the hydrodynamic destabilization of an initially stable stratification when an $A + B \rightarrow$ oscillator reaction provides the engine for dynamic localized periodic variations of the density in space and time. Reaction-diffusion-convection (RDC) interplay has already been thoroughly investigated for oscillatory systems when the initial reactants of the oscillatory reaction are homogeneously distributed in the reactor, showing that RD structures can be deformed and accelerated by convective flows (see Refs. 34 and 35 and references therein). The RDC interplay has also been demonstrated to be at the basis of order-disorder transition in the BZ oscillator.³⁶

Here, we focus on a double-layer system to show the conditions in which the chemically mediated buoyancy forcing sustained by an oscillator induces (i) pulsatile convective flows and (ii) transverse breaking of symmetry due to RD mechanisms (typically a Turing instability) coupling/competing with hydrodynamics. So far, oscillatory and travelling fingering has been for instance observed in immiscible or partially miscible vertical double-layer systems, triggered by Marangoni effects due to the mass transfer from the top to the bottom layer or induced by a chemical reaction locally producing a surfactant.^{31,37,38} A single example of pulsatile hydrodynamic structures promoted by an oscillatory chemical source in double layer miscible systems has been reported only recently³⁹ in experiments where two solutions each containing a subpart of the oscillating BZ^{6,7} reaction are put in contact in the gravity field.

In this context, our objective is to give, *via* a numerical study of the Brusselator model, an overview of the possible chemo-hydrodynamic scenarios in $A + B \rightarrow$ oscillator systems that can provide an interpretative framework for RDC

dynamics already observed, but also inspire new experiments in the search for new patterns.

The article is organized as follows: in Sec. II, we introduce the RDC model describing the development of the Brusselator kinetics in the presence of diffusive and convective transport in a localized reaction zone upon contact along a given interface between two solutions each containing a different initial reactant of the chemical oscillator. In Sec. III, we analyse the spatio-temporal evolution of one-dimensional profiles of the species concentrations and of the density, allowing us to predict qualitative features of the chemo-convective instabilities that can develop depending on the species contribution to the density. In Sec. IV, we show spatio-temporal dynamics obtained from numerical simulations of the full RDC model in two spatial dimensions. We discuss these scenarios in relation to their density profiles and characterize their main features. A concluding discussion is drawn in Sec. V.

II. MODEL

We consider a two-dimensional system in the reference frame (y, z) , in which z points upwards against the gravitational field \mathbf{g} and y is the horizontal axis. In this vertical set-up, we analyzed a two-layer configuration in which the pools of miscible reactants A (with density ρ_A) and B (with density ρ_B) of the Brusselator are initially separated along a horizontal line located at $z = z_0 = L_z/2$ (see Fig. 1). This stratification is assumed to be initially buoyantly stable (i.e., $\rho_B > \rho_A$). There are initially no intermediate species X and Y such that the initial condition reads

$$(A, B, X, Y) = (A_0, 0, 0, 0) \text{ (Side-1) for } z \geq z_0 = L_z/2, \forall y, \quad (2)$$

$$(A, B, X, Y) = (0, B_0, 0, 0) \text{ (Side-2) for } z \leq z_0 = L_z/2, \forall y. \quad (3)$$

We define $\beta = B_0/A_0$ as the ratio between the initial concentrations B_0 and A_0 of reactants B and A , respectively and, since in our simulations we will use $A_0 = 1$, we have $\beta = B_0$.

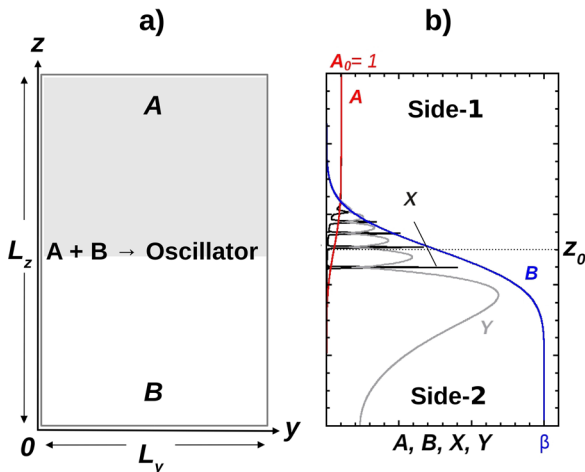


FIG. 1. (a) Schematic of the two-dimensional $A + B \rightarrow$ oscillator system under analysis. (b) Example of RD spatial profiles of the Brusselator chemical species (A, B, X, Y) after solutions A and B start mixing.

Upon diffusive mixing and reaction between the two reactants A and B , some nonlinear dynamics involving the intermediate species X and Y start to develop in time across the initial contact line. These spatio-temporal dynamics are governed by a set of partial differential equations in which the chemical kinetics is coupled to fickian diffusion and to natural convection described by Stoke's equations as

$$\partial_t A + (\mathbf{u} \cdot \nabla) A = D_A \nabla^2 A - k_1 A, \quad (4)$$

$$\partial_t B + (\mathbf{u} \cdot \nabla) B = D_B \nabla^2 B - k_2 B X, \quad (5)$$

$$\partial_t X + (\mathbf{u} \cdot \nabla) X = D_x \nabla^2 X + k_1 A - k_2 B X + k_3 X^2 Y - k_4 X, \quad (6)$$

$$\partial_t Y + (\mathbf{u} \cdot \nabla) Y = D_y \nabla^2 Y + k_2 B X - k_3 X^2 Y, \quad (7)$$

$$\partial_t D + (\mathbf{u} \cdot \nabla) D = D_D \nabla^2 D + k_2 B X, \quad (8)$$

$$\partial_t E + (\mathbf{u} \cdot \nabla) E = D_E \nabla^2 E + k_4 X, \quad (9)$$

$$\nabla p = \mu \nabla^2 \mathbf{u} - \rho(A, B, X, Y, D, E) \mathbf{g}, \quad (10)$$

$$\nabla \cdot \mathbf{u} = 0, \quad (11)$$

where $\mathbf{u} = (u, v)^T$ is the velocity field and p is the pressure. The dynamic viscosity μ , molecular diffusion coefficients D_J of species J , and acceleration due to gravity $\mathbf{g} = |\mathbf{g}|$ are assumed constant. Following a previously used parameter setting,²⁵ we consider that the main reactants, products and the autocatalytic species have similar diffusion coefficients $D_A \sim D_B \sim D_D \sim D_E \sim D_x = D$ while the so-called inhibitor Y diffuses faster to allow for the possibility of observing a Turing instability. We take here $D_y = 10D$. The hydrodynamic equations are written in the Boussinesq approximation, assuming that reaction-driven density changes only affect the gravitational term $\rho(A, B, X, Y, D, E) \mathbf{g}$ of Eq. (10) where $\rho(A, B, X, Y, D, E)$ is the density of the solution depending on the concentration of all chemical species present in the system. The concentrations are assumed small enough so that the density ρ can be expressed as a linear combination of the concentration fields according to the state equation

$$\rho(A, B, X, Y, D, E) = \rho_0 \left(1 + \sum_J \alpha_J J \right), \quad (12)$$

where ρ_0 is the density of the solvent and $\alpha_J = \frac{1}{\rho_0} \frac{\partial \rho}{\partial J}$ is the solutal expansion coefficient of the J -th species with concentration J , with $J \in \{A, B, X, Y, D, E\}$.

Following a standard scaling of the variables for the Brusselator RD equations (see Refs. 5 and 11), we introduce the set of scaled variables $\{\tilde{t} = t/t_c, (\tilde{y}, \tilde{z}) = (y, z)/l_c, \tilde{A} = A/\bar{A}; \tilde{B} = B/\bar{B}; \tilde{X} = X/\bar{X}; \tilde{Y} = Y/\bar{Y}, \tilde{D} = D/\bar{D}, \tilde{E} = E/\bar{E}, \tilde{\mathbf{u}} = \mathbf{u}/u_c, \tilde{\nabla} \tilde{p} = \tilde{\nabla} p/p_c - \rho_0 l_c \mathbf{g}/p_c\}$, where $t_c = 1/k_4$ is the reaction time scale, $l_c = \sqrt{D t_c}$ is the reaction-diffusion characteristic length, and $u_c = l_c/t_c = \sqrt{D/t_c}$, $p_c = \mu/t_c$ and $\{\bar{A} = \sqrt{k_4^3/k_1^2 k_3}, \bar{B} = \bar{D} = (k_4/k_2), \bar{X} = \bar{Y} = \bar{E} = \sqrt{k_4/k_3}\}$ are the velocity, the pressure, and the concentration scales, respectively. We also define a dimensionless density $\tilde{\rho} = (\rho - \rho_0)/\rho_c$, where $\rho_c = p_c/(l_c g)$. Introducing the stream-function, Ψ , and vorticity, ω , related to the velocity field as $u = \partial_z \Psi$, $v = -\partial_y \Psi$ and $\omega = \nabla \times \mathbf{u}$, the model can then be written in the dimensionless form

$$\partial_t A + \partial_z \Psi \partial_y A - \partial_y \Psi \partial_z A = \nabla^2 A - k_a A, \quad (13)$$

$$\partial_t B + \partial_z \Psi \partial_y B - \partial_y \Psi \partial_z B = \nabla^2 B - k_b B X, \quad (14)$$

$$\partial_t X + \partial_z \Psi \partial_y X - \partial_y \Psi \partial_z X = \nabla^2 X + A - (B+1)X + X^2 Y, \quad (15)$$

$$\partial_t Y + \partial_z \Psi \partial_y Y - \partial_y \Psi \partial_z Y = \delta \nabla^2 Y + B X - X^2 Y, \quad (16)$$

$$\partial_t D + \partial_z \Psi \partial_y D - \partial_y \Psi \partial_z D = \nabla^2 D + k_b B X, \quad (17)$$

$$\partial_t E + \partial_z \Psi \partial_y E - \partial_y \Psi \partial_z E = \nabla^2 E + X, \quad (18)$$

$$\nabla^2 \omega = \sum_J R_J \partial_y J \quad \forall J \in \{A, B, X, Y, D, E\}, \quad (19)$$

$$\nabla^2 \Psi = -\omega, \quad (20)$$

where $k_a = k_1/k_4$ and $k_b = k_2/\sqrt{k_3 k_4}$, $\delta = D_Y/D = 10$ and, for convenience, the tildes have been dropped. The solutal Rayleigh number of the J -th species, R_J , is defined as³²

$$R_J = \frac{\alpha_J \bar{J} g_c^3}{\nu D}, \quad (21)$$

where $\nu = \mu/\rho_0$ is the kinematic viscosity of the solvent and \bar{J} is the concentration scale of the J -th species. These Rayleigh numbers quantify the solutal contribution of each chemical species to buoyancy-driven flows, as they relate the dimensionless density of the solution to the concentration fields according to

$$\rho(A, B, X, Y, D, E) = \sum_J R_J J. \quad (22)$$

In the model, the rate of reactant depletion can be controlled by means of the kinetic parameters k_a and k_b . When the autocatalytic process and the consumption of the autocatalytic species are much faster than the reactant depletion steps (in other terms when $k_1 \ll k_4$ and $k_2 \ll \sqrt{k_3 k_4}$) the system, though closed, can maintain far-from-equilibrium chemical conditions and k_a and k_b can be neglected during some time. This condition is experimentally possible in chemical oscillators and is typically encountered in the BZ system, where oscillations and RD structures persist in quasi-stationary conditions quite a long time in batch reactors before evolving to equilibrium. For the BZ system, we have recently shown that numerical simulations of an analogous two-layer system carried out by using the Oregonator model without reactant consumption compare favourably with the spatio-temporal dynamics found in the corresponding experiments.⁴⁰ On the basis of this evidence, we assume here that $k_a = k_b = 0$.

Equations (13)–(20) are solved numerically by using the Alternating Direction Implicit Method (ADI).^{32,41} In our simulations, we consider a rectangular domain of dimensionless width $L_y = 400$ and height $L_z = 200$, discretized over a grid of 800×400 points (i.e., we use an integration space step $h_y = h_z = 0.5$). We apply no-flux boundary conditions for all the concentration fields of the chemical species at the boundaries of the simulation domain. No-slip conditions are required at rigid walls for the velocity field³² (i.e., $\Psi = 0$). Simulations are run using the integration time step $h_t = 1 \times 10^{-3}$.

III. DENSITY PROFILES

Possible chemo-hydrodynamic scenarios in the $A + B \rightarrow$ Brusselator system can be qualitatively predicted by analysing the morphologies of the one-dimensional density profiles along the gravitational axis z . These profiles can be reconstructed from the reaction-diffusion concentration fields³⁸ [i.e., solutions of Eqs. (13)–(18) with $\Psi = 0$] thanks to the state equation Eq. (22), and allow us to single out the possible formation of local areas featuring unfavourable density gradients (e.g., denser fluid overlying less dense fluid or *vice versa*) responsible for buoyancy-driven convective instabilities.

Let us then first focus on the dynamical evolution of RD concentration profiles. The main reactants A and B of the Brusselator evolve according to the analytical form

$$A(y, z, t) = \frac{1}{2} \operatorname{erfc} \left(-\frac{(z - z_0)}{\sqrt{4t}} \right), \quad (23)$$

$$B(y, z, t) = \frac{\beta}{2} \operatorname{erfc} \left(\frac{(z - z_0)}{\sqrt{4t}} \right), \quad (24)$$

describing the diffusive smoothing of the initial step function distributions.

In our previous work,²⁵ we showed that, for the species X and Y concentration profiles, there are two possible RD scenarios depending on the values of the diffusion ratio δ and of β . The first one occurs if

$$\beta < F(\delta, A_0), \quad (25)$$

where

$$F(\delta, A_0) = \frac{A_0(\delta + 1)^2}{(\delta - 1)(2\sqrt{\delta} + A_0(\delta - 1))} \\ \forall \delta < \left(\frac{\sqrt{1 + A_0^2} - 1}{A_0} \right)^2 \text{ and } A_0 > 0. \quad (26)$$

This regime is characterized by the formation of traveling pulses of X and Y that emerge below the initial contact line, move towards Side-2, and vanish at the border of the region controlled by the Hopf instability.²⁵ This dynamics is summarized in Figs. 2(a) and 2(b) describing the spatio-temporal evolution of the Brusselator intermediates X and Y .

A second scenario, parametrically defined by condition

$$\beta > F(\delta, A_0), \quad (27)$$

shows coexisting and spatially adjacent Hopf and Turing regimes. In Figs. 3(a) and 3(b), quasi-stationary structures of the intermediates start forming in the region where the Turing instability locally induces a transverse breaking of symmetry. These structures experience in time a drifting towards the bottom side as soon as they approach the region where conditions for Hopf and Turing instabilities are simultaneously met (CTH point).²⁵

In the most studied $A + B \rightarrow C$ case, the formation of a chemical front of the product C across the reactive area leads to asymptotically self-similar density profiles with no possible transverse symmetry breaking or temporal oscillations.³³

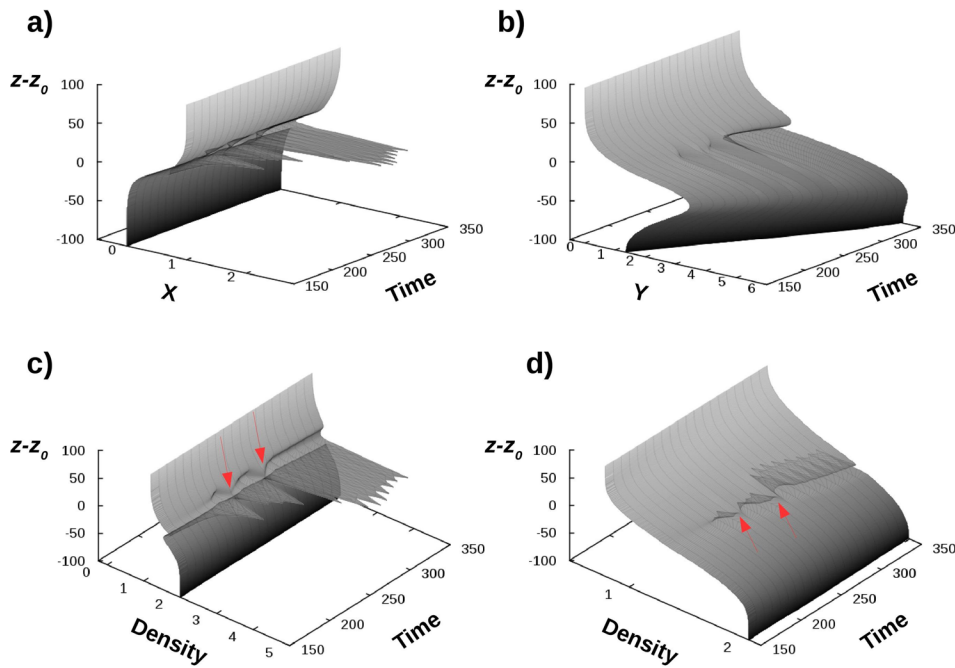


FIG. 2. Hopf-dominated RD spatio-temporal behaviour of the Brusselator intermediates X (a) and Y (b) in the $A + B \rightarrow$ Oscillator configuration ($A_0 = 1, B_0 = 2$). Spatio-temporal density profiles for X contributing positively [$R_X = 1.2$, panel (c)] and negatively [$R_X = -0.2$, panel (d)] to the density. In (c) $R_A = 0, R_B = 1$ while $R_A = 1, R_B = 1$ in (d). $z - z_0 = 0$ represents the initial position of the interface.

By contrast, the oscillatory kinetics coupled to diffusion can sustain periodical changes in the concentration of the chemical intermediates both in time and space, and hence pulsating density profiles can provide the engine for a buoyancy-driven destabilization of initially stable stratifications (i.e., $\rho_A < \rho_B$) as well as for new chemo-hydrodynamic patterns.

To simplify the system, we assume that the reaction products D and E negligibly contribute to density changes ($R_D \sim R_E \sim 0$). Moreover, we consider that the oscillatory X -species intermediate dominates dynamical and local density variations due to the reaction and pose $R_Y \sim 0$. This is in line with what is found experimentally with the BZ reaction,^{42–44} where density changes are mainly determined by

the periodic transformation of the catalyst from the reduced into its denser oxidized form. This choice is further motivated by the fact that, in the model dynamics, X is the species that features a localized oscillatory behaviour close to the interfacial area, while Y pulses are preceded by a leading diffusion-limited front propagating towards the bottom layer [see both Figs. 2(b) and 3(b)]. Since $D_X = D_A = D_B = D$, we avoid the occurrence of possible differential diffusion convective effects.

In the Hopf-dominated RD case, chemical pulses of the intermediate X are exploited to induce a periodic buoyancy forcing across the initial interface both when X contributes positively ($R_X > 0$) or negatively ($R_X < 0$) to the density. In Figs. 2(c) and 2(d), we show two examples of possible

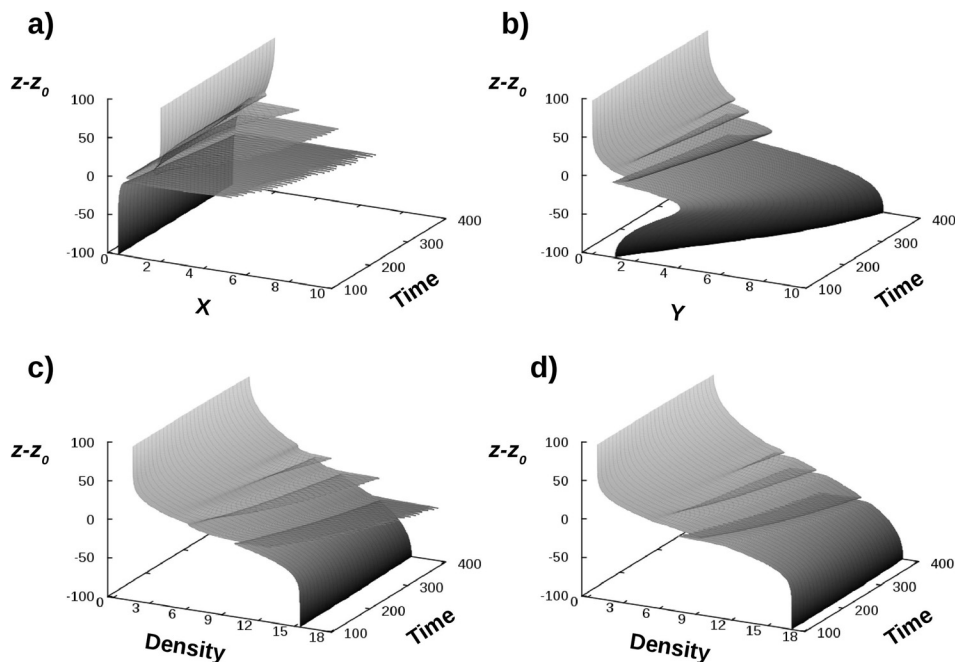


FIG. 3. Turing-Hopf-dominated RD spatio-temporal behaviour of the Brusselator species X (a) and Y (b) in the $A + B \rightarrow$ oscillator configuration ($A_0 = 1, B_0 = 15$). Corresponding spatio-temporal density profiles for X contributing positively [$R_X = 0.8$, panel (c)] and negatively [$R_X = -0.2$, panel (d)] to the density. In (c) $R_A = 0, R_B = 1$ while $R_A = 1, R_B = 1.1$ in (d). $z - z_0 = 0$ represents the initial interface.

shapes of the related density profiles. Panel (a) illustrates the spacetime evolution in the morphology of the density profile when R_X is positive. We can observe a periodic formation of a steep density maximum corresponding to the emergence of new concentration pulses in X which, at the beginning, are periodically “absorbed” in the downwardly increasing density profile [see arrows in Fig. 2(c)]. In time, the intensity of these pulsed density maxima as well as the period by which they form increase and the system is then expected to switch to a persistent convective instability. A symmetrical scenario is found when negative values for R_X are considered. In Fig. 2(d), we can follow a typical evolution of the density profile with $R_X < 0$. In both examples, the periodic occurrence in time of the density extrema is expected to sustain in the gravitational field pulsatile fingering or plumes.

In the scenario where both Hopf and Turing modes coexist, quasi-stationary bands emerging in the concentration profile of X [see Fig. 3(a)] result in density maxima if X contributes positively to the density and in density minima in the opposite case. These density profiles, plotted as a function of the time in Figs. 3(c) and 3(d), respectively, suggest the possible formation of buoyancy-driven sinking or rising structures.

IV. REACTION-DIFFUSION-CONVECTION PATTERNS

The qualitative information extracted from the morphology of the density profiles can be compared to the spatio-temporal dynamics obtained from the nonlinear simulations of the full equation system (13–20) for the general cases considered above. An overview of these chemo-hydrodynamic patterns is presented in Fig. 4. Following the discussion in Sec. III, this parameter space classifies the possible dynamics on the basis of the inherent RD case (controlled here by B_0 with $\delta = 10$) and of the contribution of X to the density profile (controlled by R_X). We can identify four regions. Two of them correspond to the Hopf-dominated dynamics with $R_X > 0$ (*pulsatile sinking fingering*) and $R_X < 0$ (*pulsatile rising plumes*). The two other ones are obtained when the Turing instability also comes into play. We can then find Turing spots, respectively, sinking ($R_X > 0$, Turing rain) or rising ($R_X < 0$, Turing bubbling) in the gravitational field. Let us now provide a detailed description and characterization of the associated spatio-temporal dynamics.

A. Hopf-dominated dynamics, $R_X > 0$

The phenomenology of this scenario is illustrated in the spacetime plot of density [Fig. 5(a)] featuring the dynamics of the representative finger framed by the red box of Fig. 4. There is an initial periodic formation of planar fronts, moving from Side-1 to the bottom layer, within the expanding region dominated by the Hopf instability. As described in Sec. III, for $R_X > 0$ these fronts feature a pulsatile buoyancy forcing that destabilizes the initially stable stratification ($R_A = 0, R_B = 1$). In time, the planar front deforms into fingers. As observed in the evolution of the density profiles, during the first stages of the instability, some density maxima form and vanish, thus activating and suppressing the driving force of the buoyancy-driven hydrodynamic instability. As a consequence, convective fingers form, grow, and

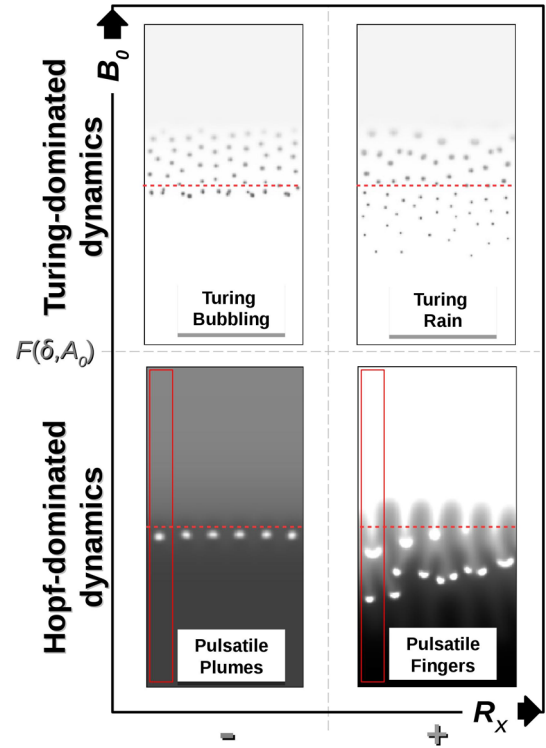


FIG. 4. Classification in the parameter space (B_0, R_X) of the buoyancy-driven chemo-hydrodynamic scenarios observed in the $A + B \rightarrow$ Brusselator system. Red boxes frame a selection of the spatial domain used to build the spatio-temporal plots of the system, while the horizontal red dashed lines locate the contact line between the two initial layers. The threshold $F(\delta, A_0)$ is described by Eq. (26).

then smooth-down by spreading in the bottom layer. This mechanism results in a transient oscillatory fingering, the lifespan of which decreases by increasing R_X . As a matter of fact, the amplitude of the concentration pulsations in the chemical intermediate X then increases in time and the corresponding density maxima, though showing an oscillatory dynamics, cannot be “absorbed” any more in the downwardly increasing density profile. The convective fingers appear then persistently and experience pulsations at their tip inducing new pulses. These follow pre-existing convective currents giving rise to segmented fingering patterns.

In order to show the occurrence of oscillatory fingers close to the interface, we plot in Fig. 5(b) the temporal evolution of the velocity field at $y = 20, z = L_z/2$, which is the small square shown in the first frame of the space-time plot of Fig. 5(a). When convection sets-in (after around 280 time units), both velocity components show an oscillatory behaviour indicative of the pulsatile nature of the flow. A further quantitative evidence of the oscillatory fingering is given by plotting the extension of the convective area, L , as a function of time [Fig. 5(d)]. To compute L , we consider the vorticity profile, $\omega(y, z, \tau)$ transversely averaged over the y -direction

$$\langle \omega \rangle(z, t) = \frac{1}{L_y} \int_0^{L_y} \omega(y, z, t) dy, \quad (28)$$

and localize tip points of the convective area as the top and the bottom positions where $\langle \omega \rangle(z, \tau)$ becomes less than 0.01. In Fig. 5(d), we can appreciate how $L(t)$ undergoes after a

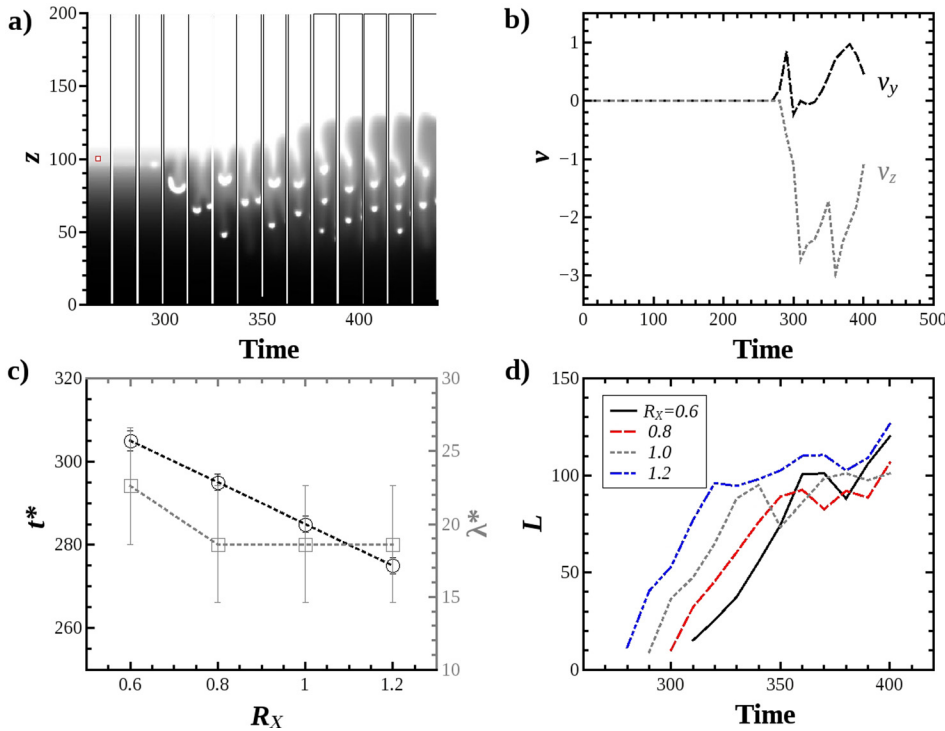


FIG. 5. (a) Spatio-temporal dynamics of a representative finger of the pulsatile fingering scenario ($A_0 = 1, B_0 = 2$) obtained for $R_X = 1.2, R_A = 0, R_B = 1$. (b) Temporal evolution of the velocity components v_y and v_z at the interfacial check point ($y = 20, z = L_z/2$) [see the box in the first snapshot of panel (a)]. (c) Instability onset time t^* and related wavelength λ^* as a function of R_X . (d) Temporal evolution of the mixing length $L(t)$ for $R_X \in [0.6, 1.2]$.

while an oscillatory trend in correspondence of the oscillatory fingering. This is different from the standard $A + B \rightarrow C$ cases where $L(t)$ follows a smooth linear growth in the convective regime. Note that, by increasing R_X , convection starts earlier and spreads faster.

Finally, in Fig. 5(c), we characterize the dependence of the onset time of the convective instability, t^* , (defined as the time at which fingers appear in the concentration fields) and the characteristic wavelength at convection onset, λ^* , as a function of R_X . As expected, since R_X controls the magnitude of the destabilizing density maxima, t^* decreases when increasing R_X , but the effect on λ^* is not dramatic in the range considered.

B. Hopf-dominated dynamics, $R_X < 0$

The RD dynamics associated with this scenario is similar to the previous case, but since here X is locally decreasing the density, we can observe the formation of rising plumes after a given induction period. Once more, in Fig. 6(a), we capture the spatio-temporal dynamics by following a representative portion of the spatial domain (see red box in Fig. 4) as a function of time. As soon as the hydrodynamic instability breaks the transverse symmetry, the resulting chemical drops rise in the gravitational field and sink again when the density depletion is overcome. This dynamics results in chemical spots following a circular trajectory across the reactive zone as detailed in Fig. 7.

Consistently, the flow is characterized in this region by an oscillatory velocity profile in time, as seen in Fig. 6(b) giving the temporal evolution of the horizontal and the vertical component of the velocity field at the point $y = 20, z = L_z/2$, i.e., the red square of the first snapshot of Fig. 6(a). The convective lengths $L(t)$ for values of $R_X \in [-0.6, -0.2]$, plotted

in Fig. 6(d), similarly show a non-monotonic and oscillatory behaviour. The onset time and the wavelength of the pattern are only slightly affected when R_X is varied in the range $[-0.6, -0.2]$.

C. Turing-dominated dynamics

The dynamics changes drastically when quasi-stationary Turing structures can locally develop. In the two-dimensional double-layer configuration under analysis, the RD system can initially break the transversal symmetry when the Turing instability is at work. Concentration spots are then seen to form close to the reactive interface. In the gravitational field, the emerging array of spots becomes hydrodynamically unstable⁴⁵ and these concentration dots start then falling down if $R_X > 0$, slaved to the local velocity field that they themselves induce. The spatial distribution of this *Turing rain* pattern is characterized by a shorter wavelength than the one of the pure RD analogues [cfr Fig. 8(a) vs Fig. 8(b)]. This might be due to the enhanced mixing by convection at the interface which changes the local concentration of reactant A controlling the pattern wavelength as $\lambda^2 = 4\pi^2(\sqrt{D_X D_Y})/A(y, z, t)$. The chemical spots decrease their size when going downward the z -axis, as they progressively homogenize in the bottom layer where the concentration of X is initially equal to zero. In Fig. 9 (black solid lines), we track the temporal evolution of the vertical extent of this RDC Turing rain by plotting the temporal evolution of the location of the upper and the lower extremes of the zone embedding the chemical spots. Due to the formation of locally denser zones, the chemo-hydrodynamic pattern extends more downwards in the bottom layer with respect to the related RD dynamics (blue dotted lines).

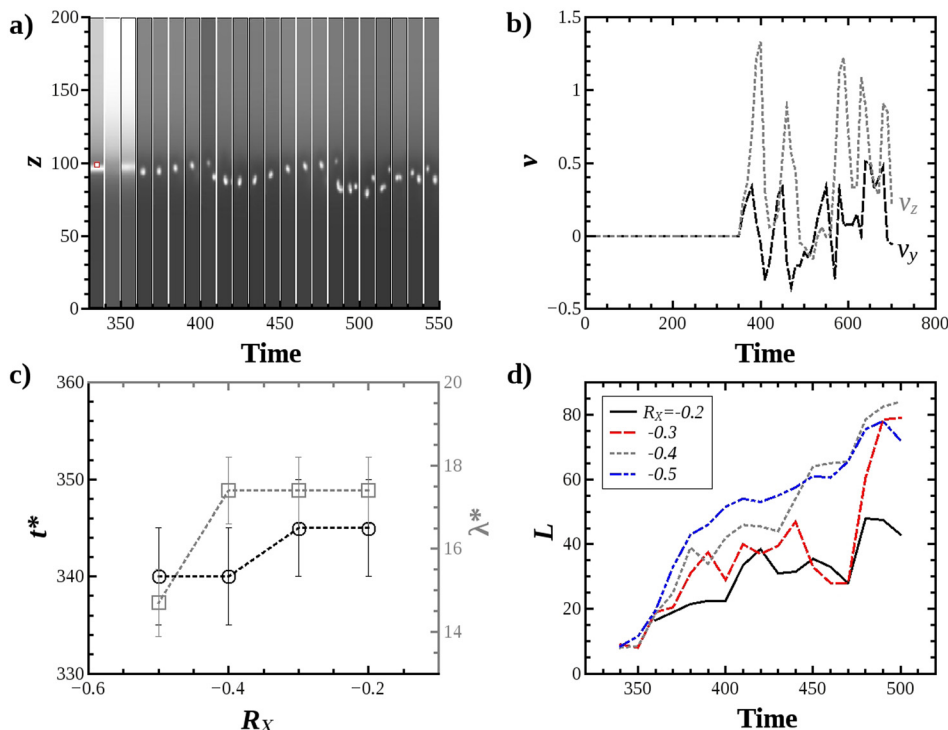


FIG. 6. (a) Spatio-temporal dynamics of a representative plume of the pulsatile plume scenario ($A_0 = 1, B_0 = 2$) for $R_X = -0.2, R_A = 1, R_B = 1$. (b) Temporal evolution of the two velocity components at the interfacial check point ($y = 20, z = L_z/2$) [see the red box in the first snapshot of panel (a)]. (c) Instability onset time t^* and related wavelength λ^* as a function of R_X . (d) Temporal evolution of the mixing length L for $R_X \in [-0.6, -0.2]$.

A reverse behaviour is obtained for negative values of R_X as shown in Fig. 8(c). In this case, Turing spots behave like bubbles (*Turing bubbling*) rising in the gravitational field. Spots form at preferential nucleation points along the initial two-layer contact line [see arrows in panel (c)] and tend to follow the upward paths traced by previous spots. As a result, they are arranged and characterized by a new wavelength as compared to the RD pattern. As can be observed in Fig. 9 (dashed red lines), the pattern develop asymmetrically towards the top layer, while the downward growth of the

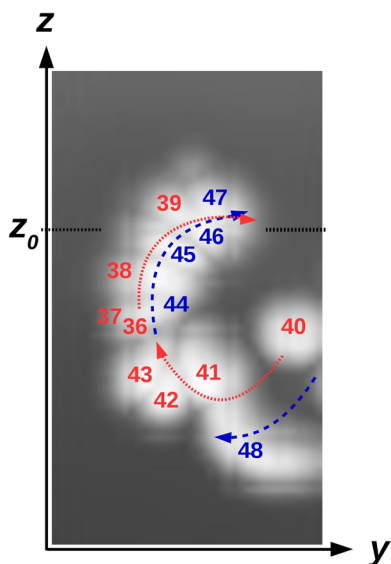


FIG. 7. Detailed illustration of the circular motion of chemical spots in the dynamics shown in Fig. 6(a). The image stacks and superimposes consecutive snapshots zoomed across the initial interface ($z \in [50, 120], y \in [0, 20]$) in the time interval.^{36,48} Red and blue numbers along the dashed and the dotted-dashed arrows trace the first (36–43 time units) and the second (44–48 time units) cycle, respectively.

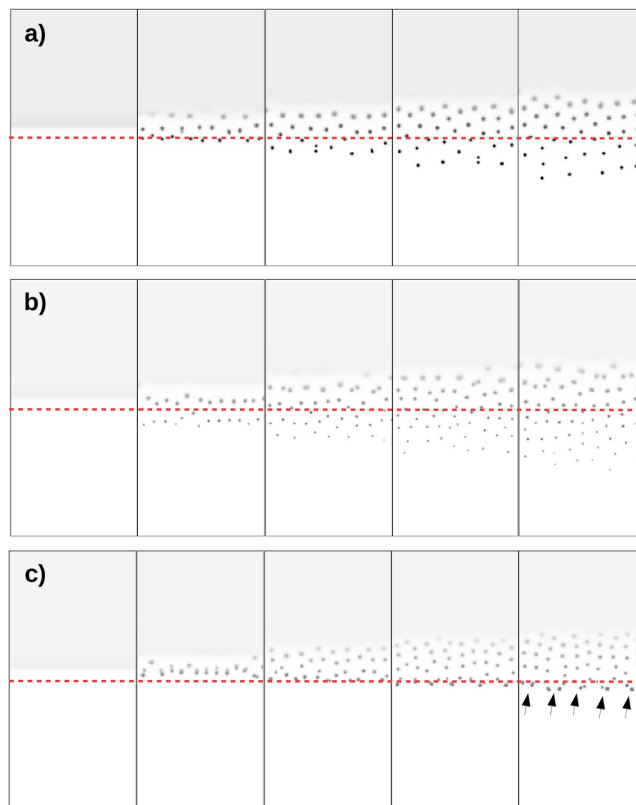


FIG. 8. Spatio-temporal evolution of chemical patterns (concentration field of species X) when the Hopf and the Turing domains coexist in the $A + B \rightarrow$ Brusselator system ($A_0 = 1, B_0 = 15$). Panel (a) shows the formation of Turing spots in the convection-free system ($R_X = 0$), while panels (b) and (c) sketch the pattern development for positive and negative R_X (0.8 and -0.2), respectively. The arrows in panel (c) indicate the nucleation points of Turing spots at the interface. The horizontal red dashed lines locate the position of the initial contact line between the two reactant layers.

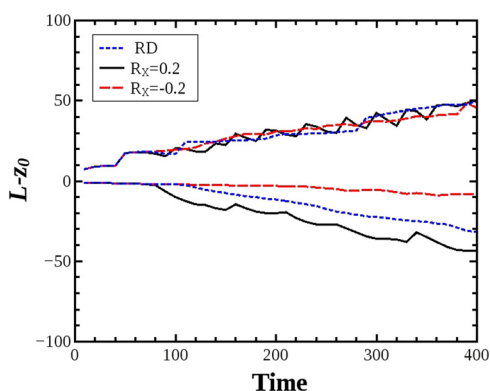


FIG. 9. Temporal evolution of the vertical length of the chemo-hydrodynamic patterns in the Hopf-Turing regime.

pattern is very slow. Also note that, though convection is at play, the upward evolution of the pattern occurs on similar time and space scales as the RD dynamics. Both for positive and negative R_X , when increasing the absolute value of R_X , the intensity of the local convection intensifies, thus leading to more complex and disordered dynamics.

V. CONCLUDING DISCUSSION

We have here extended the analysis of the widely studied buoyancy-driven convective instabilities of $A + B \rightarrow C$ systems to the more complex class of $A + B \rightarrow$ oscillator reactions, in which reaction intermediates present an oscillatory dynamics.

This nonlinear process occurs at the interface between two layers containing separately two different reactants of the chemical oscillator. The destabilizing effect of the reaction is studied for two cases. In the first case, the RD dynamics features a Hopf instability and oscillatory intermediates form homogeneously along the initial contact line between the layers. In the second case, the RD dynamics induces a local transversal symmetry breaking via the formation of transient Turing structures. These two scenarios were recently shown to be the only RD dynamics possible for the system under analysis.²⁵ Guided by the properties of these RD dynamics and of the associated density profiles along the gravitational field, we show that, in the absence of gels, new chemo-hydrodynamic scenarios such as pulsatile convective flows can develop. In order to point out the role of a periodic chemical forcing, we considered that only one oscillatory intermediate species can change the local density. We found that four spatio-temporal dynamics are possible depending whether the Hopf or the Turing instability initially develops across the reactive area and, for each of them, whether the oscillatory intermediate locally increases or decreases the density.

When the Hopf instability rules the dynamics, a hydrodynamic transverse destabilization of the initial interface can be observed due to the periodic formation and annihilation of density maxima ($R_X > 0$) or minima ($R_X < 0$). As a result, oscillatory and pulsatile fingers or plumes are promoted, respectively. The experimental identification of some of these scenarios could be achieved by studying in a Hele-

Shaw cell a photo-sensitive BZ oscillator.⁴⁶ This would allow to locally activate the oscillatory mechanism by a different irradiation through the excitable medium. The interface of an initially buoyantly stable stratification of the two reactant pools could be then periodically forced by means of an external pulsed and collimated light. Similarly, photochromic species giving a transition between structural isomers with different densities when irradiated could be suitably exploited in this context, by imposing external periodic irradiation of the double-layer system at the interface. Based on a similar concept, chemo-convective oscillations have been devised.⁴⁷

In the Hopf domain, we can also obtain RD waves that travel transversely along the reactive zone.²⁵ In this case, travelling fingers or plumes can be expected, provided that the waves locally increase or decrease the solution density. Such a kind of dynamics has been observed with the Belousov-Zhabotinsky reaction carried out in a double-layer configuration.^{39,48} In this system, oxidized waves moving horizontally along the reactive interface couple to vertically growing fingers induced by *in-situ* buoyancy chemical forcing.

When a reaction-diffusion Turing mechanism triggers a transversal break of symmetry and spots form across the reactive interface, *Turing rain* or *Turing bubbling* dragged by the spot-wise chemically driven velocity field can then occur depending whether $R_X > 0$ or $R_X < 0$. Note that, in this case, when the absolute value of R_X is increased, a transversal breaking of symmetry due to a hydrodynamic instability may occur first and the spatio-temporal dynamics is then closer to the pulsated fingering observed in the Hopf-dominated regime. The possibility for these scenarios could be explored by using the BZ reaction in a micellar medium, where conditions for different morphologies of the Turing structures can be obtained.

A possible extension of this theoretical investigation should include the contribution of the second chemical intermediate Y to the density and, hence, its synergetic interplay with X in the convective dynamics. Similar studies should also be developed to take into account possible reaction-driven viscosity changes in autocatalytic systems. This should allow for the uncovering of new chemo-hydrodynamic patterns and dissipative structures merging the complexity of both convective and RD patterns.

ACKNOWLEDGMENTS

M.A.B. acknowledges financial support from FRS-FNRS. A.D. acknowledges support from FRS-FNRS for the FORECAST project.

¹P. Glansdorff and I. Prigogine, *Thermodynamics of Structure, Stability and Fluctuations* (Wiley, New York, 1971).

²G. Nicolis and I. Prigogine, *Self-Organization in Nonequilibrium Systems* (Wiley, New York, 1977).

³I. Prigogine and R. Lefever, "Symmetry breaking instabilities in dissipative systems. II," *J. Chem. Phys.* **48**, 1695–1700 (1968).

⁴R. Lefever and G. Nicolis, "Chemical instabilities and sustained oscillations," *J. Theor. Biol.* **30**, 267–284 (1971).

⁵R. Lefever, G. Nicolis, and P. Borckmans, "The Brusselator: It does oscillate all the same," *J. Chem. Soc., Faraday Trans.* **1** **84**, 1013–1023 (1988).

- ⁶B. P. Belousov, "A periodic reaction and its mechanism," in *Sbornik Referatov Po Radiatsionno Meditsine* (Medgiz, Moscow, 1958), pp. 145–147.
- ⁷A. N. Zaikin and A. M. Zhabotinsky, "Concentration wave propagation in two-dimensional liquid-phase self-oscillating system," *Nature* **225**, 535–537 (1970).
- ⁸V. Castets, E. Dulos, J. Boissonade, and P. De Kepper, "Experimental evidence of a sustained standing Turing-type nonequilibrium chemical pattern," *Phys. Rev. Lett.* **64**, 2953–2956 (1990).
- ⁹A. De Wit, "Spatial patterns and spatiotemporal dynamics in chemical systems," *Adv. Chem. Phys.* **109**, 435–513 (1999).
- ¹⁰M. Hershkowitz-Kaufman and G. Nicolis, "Localized spatial structures and nonlinear chemical waves in dissipative systems," *J. Chem. Phys.* **56**, 1890–1895 (1972).
- ¹¹J. Boissonade, "Stationary structure induced along a reaction-diffusion front by a Turing symmetry breaking instability," *J. Phys. France* **49**, 541–546 (1988).
- ¹²G. Dewel and P. Borckmans, "Effects of slow spatial variations on dissipative structures," *Phys. Lett. A* **138**, 189–192 (1989).
- ¹³P. Borckmans, A. De Wit, and G. Dewel, "Competition in ramped Turing structures," *Phys. A: Stat. Mech. Appl.* **188**, 137–157 (1992).
- ¹⁴G. Dewel, P. Borckmans, A. De Wit, B. Rudovics, J.-J. Perraud, E. Dulos, J. Boissonade, and P. De Kepper, "Pattern selection and localized structures in reaction-diffusion systems," *Physica A* **213**, 181–198 (1995).
- ¹⁵I. Lengyel, S. Kádár, and I. R. Epstein, "Quasi-two-dimensional Turing patterns in an imposed gradient," *Phys. Rev. Lett.* **69**, 2729–2732 (1992).
- ¹⁶E. Dulos, P. Davies, B. Rudovics, and P. De Kepper, "From quasi-2D to 3D Turing patterns in ramped systems," *Physica D* **98**, 53–66 (1996).
- ¹⁷S. Setayeshgar and M. C. Cross, "Turing instability in a boundary-fed system," *Phys. Rev. E* **58**, 4485–4500 (1998).
- ¹⁸P. De Kepper, E. Dulos, J. Boissonade, A. De Wit, G. Dewel, and P. Borckmans, "Reaction diffusion patterns in confined chemical systems," *J. Stat. Phys.* **101**, 495–508 (2000).
- ¹⁹Z. Noszticzius, W. Horsthemke, W. D. McCormick, H. Swinney, and W. Y. Tam, "Sustained chemical waves in an annular gel reactor: A chemical pinwheel," *Nature* **329**, 619–620 (1987).
- ²⁰E. Dulos, J. Boissonade, and P. De Kepper, "Dynamics and morphology of sustained two-dimensional wave trains," *Physica A* **188**, 120–131 (1992).
- ²¹J.-J. Perraud, A. De Wit, E. Dulos, P. De Kepper, G. Dewel, and P. Borckmans, "One-dimensional "spirals": Novel asynchronous chemical wave sources," *Phys. Rev. Lett.* **71**, 1272–1275 (1993).
- ²²A. De Wit, D. Lima, G. Dewel, and P. Borckmans, "Spatiotemporal dynamics near a codimension-two point," *Phys. Rev. E* **54**, 261–271 (1996).
- ²³L. Yang, M. Dolnik, A. M. Zhabotinsky, and I. R. Epstein, "Pattern formation arising from interactions between Turing and wave instabilities," *J. Chem. Phys.* **117**, 7259–7265 (2002).
- ²⁴J. C. Tzou, Y.-P. Ma, A. Bayliss, B. J. Matkowsky, and V. A. Volpert, "Homoclinic snaking near a codimension-two Turing-Hopf bifurcation point in the Brusselator model," *Phys. Rev. E* **87**, 022908 (2013).
- ²⁵M. A. Budroni and A. De Wit, "Localized stationary and traveling reaction-diffusion patterns in a two-layer $A + B \rightarrow$ oscillator system," *Phys. Rev. E* **93**, 062207 (2016).
- ²⁶L. Gálfi and Z. Rácz, "Properties of the reaction front in an $A + B \rightarrow C$ type reaction-diffusion process," *Phys. Rev. A* **38**, 3151–3154 (1988).
- ²⁷A. De Wit, "Chemo-hydrodynamic patterns in porous media," *Philos. Trans. R. Soc. A* **374**, 20150419 (2016).
- ²⁸K. Eckert and A. Grahn, "Plume and finger regimes driven by an exothermic interfacial reaction," *Phys. Rev. Lett.* **82**, 4436–4439 (1999).
- ²⁹C. Almarcha, P. M. J. Trevelyan, P. Grosfils, and A. De Wit, "Chemically driven hydrodynamic instabilities," *Phys. Rev. Lett.* **104**, 044501 (2010).
- ³⁰C. Almarcha, Y. R'Honi, Y. De Decker, P. M. J. Trevelyan, K. Eckert, and A. De Wit, "Convective mixing induced by acid base reactions," *J. Phys. Chem. B* **115**, 9739–9744 (2011).
- ³¹K. Eckert, M. Acker, R. Tadmouri, and V. Pimienta, "Chemo-Marangoni convection driven by an interfacial reaction: Pattern formation and kinetics," *Chaos* **22**, 037112 (2012).
- ³²L. Lemaigre, M. A. Budroni, L. A. Riolfo, P. Grosfils, and A. De Wit, "Asymmetric Rayleigh-Taylor and double-diffusive fingers in reactive systems," *Phys. Fluids* **25**, 014103 (2013).
- ³³P. M. J. Trevelyan, C. Almarcha, and A. De Wit, "Buoyancy-driven instabilities around miscible $A + B \rightarrow C$ reaction fronts: A general classification," *Phys. Rev. E* **91**, 023001 (2015).
- ³⁴M. A. Budroni, M. Rustici, and E. Tiezzi, "On the origin of chaos in the Belousov-Zhabotinsky reaction in closed and unstirred reactors," *Math. Modell. Nat. Phenom.* **6**, 226–242 (2011).
- ³⁵H. Miike, T. Sakurai, A. Nomura, and S. C. Müller, "Chemically driven convection in the Belousov-Zhabotinsky reaction-evolutionary pattern dynamics," *Forma* **30**, S33–S53 (2015).
- ³⁶M. A. Budroni, M. Masia, M. Rustici, N. Marchettini, V. Volpert, and P. C. Cresto, "Ruelle-Takens-Newhouse scenario in reaction-diffusion-convection system," *J. Chem. Phys.* **128**, 111102 (2008).
- ³⁷Y. Shi and E. Kerstin, "Orientation-dependent hydrodynamic instabilities from chemo-Marangoni cells to large scale interfacial deformations," *Chin. J. Chem. Eng.* **15**, 748–753 (2007).
- ³⁸M. A. Budroni, L. A. Riolfo, L. Lemaigre, F. Rossi, M. Rustici, and A. De Wit, "Chemical control of hydrodynamic instabilities in partially miscible two-layer systems," *J. Phys. Chem. Lett.* **5**, 875–881 (2014).
- ³⁹D. M. Escala, M. A. Budroni, J. Carballido-Landeira, A. De Wit, and A. P. Muñuzuri, "Self-organized traveling chemo-hydrodynamic fingers triggered by a chemical oscillator," *J. Phys. Chem. Lett.* **5**, 413–418 (2014).
- ⁴⁰M. A. Budroni, L. Lemaigre, D. M. Escala, A. P. Muñuzuri, and A. De Wit, "Spatially localized chemical patterns around an $A + B \rightarrow$ oscillator front," *J. Phys. Chem. A* **120**, 851–860 (2016).
- ⁴¹D. W. Peaceman and H. H. Rachford, "The numerical solution of parabolic and elliptic differential equations," *J. Soc. Ind. Appl. Math.* **3**, 28 (1955).
- ⁴²J. A. Pojman and I. R. Epstein, "Convective effects on chemical waves. 1. mechanisms and stability criteria," *J. Phys. Chem.* **94**, 4966–4972 (1990).
- ⁴³M. A. Budroni, M. Masia, M. Rustici, N. Marchettini, and V. Volpert, "Bifurcations in spiral tip dynamics induced by natural convection in the Belousov-Zhabotinsky reaction," *J. Chem. Phys.* **130**, 024902 (2009).
- ⁴⁴F. Rossi, M. A. Budroni, N. Marchettini, and J. Carballido-Landeira, "Segmented waves in a reaction-diffusion-convection system," *Chaos* **22**, 037109 (2012).
- ⁴⁵D. A. Vasquez, J. W. Wilder, and B. F. Edwards, "Convective Turing patterns," *Phys. Rev. Lett.* **71**, 1538–1541 (1993).
- ⁴⁶J. N. Demas and D. Diemente, "An oscillating chemical reaction with a luminescent indicator," *J. Chem. Educ.* **50**, 357 (1973).
- ⁴⁷P. L. Gentili, M. Dolnik, and I. Epstein, "Photochemical oscillator: Colored hydrodynamic oscillations and waves in a photochromic system," *J. Phys. Chem. C* **118**, 598–608 (2014).
- ⁴⁸L. Lemaigre, "Convective patterns triggered by chemical reactions, dissolution and cross-diffusion: An experimental study," Ph.D. thesis (Université libre de Bruxelles, 2016).